Real-time component-based particle size measurement and dissolution prediction during continuous powder feeding using machine vision and artificial intelligence-based object detection

Áron Kálnai , Máté Ficzere , Brigitta Nagy , Orsolya Péterfi , Máté Benczúr , Zsombor Kristóf Nagy , Dorián László Galata

PII: S0928-0987(25)00079-X
DOI: https://doi.org/10.1016/j.ejps.2025.107080
Reference: PHASCI 107080

To appear in: *European Journal of Pharmaceutical Sciences*

Received date: 9 January 2025
Revised date: 25 February 2025
Accepted date: 19 March 2025

Please cite this article as: Áron Kálnai , Máté Ficzere , Brigitta Nagy , Orsolya Péterfi , Máté Benczúr , Zsombor Kristóf Nagy , Dorián László Galata , Real-time component-based particle size measurement and dissolution prediction during continuous powder feeding using machine vision and artificial intelligence-based object detection, *European Journal of Pharmaceutical Sciences* (2025), doi: https://doi.org/10.1016/j.ejps.2025.107080

Real-time component-based particle size measurement and dissolution prediction during continuous powder feeding using machine vision and artificial intelligence-based object detection

Áron Kálnai[1], Máté Ficzere[1], Brigitta Nagy[1], Orsolya Péterfi[1], Máté Benczúr[1], Zsombor Kristóf Nagy*[1], Dorián László Galata[1]

[1] Department of Organic Chemistry and Technology, Faculty of Chemical Technology and Biotechnology, Budapest University of Technology and Economics, H-1111 Budapest, Műegyetem rakpart 3

* Correspondence: zsknagy@oct.bme.hu; Tel.: +36 1 463 4129

Abstract

This work presents a system, in which machine vision combined with artificial intelligence-based image analysis was used to determine the component-based particle size distribution of pharmaceutical powder blends. The blends consisted of acetylsalicylic acid (ASA) and calcium hydrogen phosphate (CHP). Images of powders were recorded with a digital camera in-line during feeding from a continuous feeder. The component-based particle size distributions determined with the system correlated well with those measured using a microscope as a reference method. This novel method proved to be effective in the real-time determination of particle size distribution of different components in the same blend. It was also possible to predict the in vitro dissolution profile of capsules filled with this blend by using the measured particle size distribution of ASA as input in a population balance model. The method could provide valuable information on the blends used in the pharmaceutical industry and could play a key role in the development of pharmaceutical quality control.

Keywords

particle size measurement, machine vision, artificial intelligence, YOLOv5, dissolution prediction, population balance modelling

1. Introduction

Powder blends are integral to many areas of the pharmaceutical industry. Tablets represent up to 70% of all drugs on the market. Powder blends are the main intermediate products of tablets. Therefore, knowing and controlling their properties is of utmost importance. It's particularly important considering that the malfunctions of the equipment used in the manufacturing of tablets are mainly tied to powder behaviour [1]. The pharmaceutical excipients can vary in size from the nanoscale colloidal range to granules of millimetre size in various pharmaceutical formulations. The two most important parameters of pharmaceutical powder particles are their size and shape, since these can have a huge effect on the quality attributes of the powders and a considerable impact on the end product. Particle size can affect content uniformity since the particles of different size and shape can segregate and cause inhomogeneity. Its effect on flow properties should not be overlooked [2, 3]. Particle size can also strongly influence dissolution and absorption rates [4], especially in the case of BCS II compounds, while for BCS I/III compounds particle size distribution is not the limiting factor, making the development of the dissolution method simpler. Given this great impact, particle size is in many pharmaceutical processes considered a Critical Quality

Attribute (CQA) [5] typically measured using the distribution of parameters such as equivalent diameter or Feret diameter.

Determining and controlling the component-based particle size distributions is crucial in understanding the segregation of powder blends, where the sticking behaviour is dependent on material properties, such as surface area and crystal morphology [6]. Although there are as many as 13 mechanisms related to the segregation of ingredients identified in engineering areas [7] only a few are relevant in handling pharmaceutical solids. Amongst those the most relevant ones are sifting, fluidization and rolling. In these three phenomena the varying behaviour of the particles is attributed to the difference in their sizes, rather than the differences in the materials themselves [8]. As a result, particles of the same component but of varying sizes and shapes may exhibit different behaviours, which can lead to further segregation and inhomogeneity. In their research, Péterfi et al. have investigated the surface powder sticking of blends containing amlodipine as API, highlighting that the concentration of amlodipine increased in the material adhered to the inner wall, showing that in certain cases different materials may show diverse behaviour when contacting various surfaces [9].

Traditionally, particle size has been determined using off-line methods such as sieve analysis, laser diffraction (LD), and microscopy. These methods often require skilled operators and can be time consuming, therefore they are typically not suitable for real-time process control [5]. Recently, as Process Analytical Technology (PAT) and continuous manufacturing (CM) are becoming more widespread in the industry, there has been a significant shift towards in-line methods in particle size analysis. These methods include in-line LD [10], spatial filtering velocimetry (SFV) [11] and Focused Beam Reflectance Measurement (FBRM) [12]. LD is still mostly used as an off-line method. While LD can measure the size of relatively small, even nanoscale particles, the primary limitations of the technology are its destructivity and the fact that the particles are always assumed to be spherical. For non-spherical particles, this leads to a distribution of equivalent light scatter diameters, which is dependent on particle orientation [13]. While SFV can easily be installed into manufacturing equipment, it requires special attention and maintenance and in many cases the use of pressurised air in order to ensure representative sampling. In FBRM a major challenge in interpreting its results is that the chord length distributions measured by the method may not correlate directly with particle size [5]. Neither of the aforementioned methods are capable of differentiating between particles of varying materials, thus they are not able to determine the component-based particle size distribution of a powder blend. This leads to limitations in the application of such methods in CM.

Machine vision is a simple and effective tool for the in-line analysis of pharmaceutical processes. A machine vision system recovers useful information about a scene from its two-dimensional projections [14]. In past studies machine vision systems have been used to classify the quality of coated tablets [15], to predict bulk powder flowability of pharmaceutical materials based on their particle shape and size distributions [16] and to characterize the particle size distribution of granular products [17]. A machine vision system comprises of several components, including the camera and light source, each serving the purpose of collecting reproducible data [18]. For the light source, the most important factor is the consistency in the quality of the emitted light, which is primarily required due to the strict pharmaceutical and GMP standards. In their publication, Martin et al. provided an in-depth analysis of selecting an appropriate light source and on the importance of optimal setup in machine vision systems [19]. Selecting the appropriate camera is crucial for capturing images of the required quality, which can be utilized not only for object detection, but for determining

shapes and leveraging properties (colour, transparency etc.) to distinguish between different components [20]. A limitation of image analysis and machine vision for monitoring particle parameters during production is the low efficiency of data evaluation with classical algorithms, such as thresholding [21].

The combination of artificial intelligence and neural networks applied to the processing of information obtained through machine vision has the potential to yield significant advancements. For the automation and efficiency improvement of image analysis YOLOv5, an object detecting algorithm combined with a convolutional neural network (CNN), may prove useful. It uses a convolutional neural network to detect different objects, thereby enhancing its performance and efficiency in real-time detection. Its ability to learn many appearances of an object makes it better at managing real-world situations where the appearance of objects changes dynamically [22, 23]. Compared to the object detection algorithms used in the past, it also has the advantage of using instance segmentation instead of bounding boxes. Instance segmentation is capable of accurately following the contours of detected objects, whereas the use of bounding boxes is most effective when the primary parameter of interest is the objects' location or quality. With the use of instance segmentation, a significant improvement could be achieved in determining object size and shape, and it has already been applied in various fields, including agriculture to enhance fruit production [24]. As for its use in the pharmaceutical industry a recent study by Fazekas et al. presented a quality assurance system, where CQAs were monitored with fast at-line techniques. The developed technique measured the diameter of electrospun fibrous samples using camera images and instance segmentation performed by a trained AI model [25].

Another valuable reference is the study by Ficzere et al., who introduced a system, where object detection was used on images captured with a digital camera to simultaneously determine the API concentration and the particle size distribution of two components of a powder blend [26]. They utilized a setup where the powder blend was transferred onto a conveyor belt providing a surface to capture images with a digital camera and then the images were analysed using the method of bounding boxes.

The bioavailability of orally administered drugs depends on their absorption from the gastrointestinal tract (GI). The Biopharmaceutical Classification System (BCS) is a system used to classify drugs based on their solubility and permeability. It helps predict the rate and extent of drug absorption in the body. For drugs belonging to BCS II (characterized by high permeability and low solubility), the dissolution rate in GI fluids serves as the rate limiting step in the absorption of these drugs rather than their diffusion through the GI membrane [27]. It is therefore an integral part of preclinical and clinical development. Dissolution testing constitutes one of the most important analytical tools in the pharmaceutical industrial quality control laboratories. This analytical method typically involves numerous steps [28]. For the dissolution testing, the tablets are placed in the dissolution medium and samples are collected at predetermined time intervals for analysis of the concentration of dissolved API. This method is relatively slow, destructive, and unsuitable for examining a large number of tablets or for in-line application. Significant improvements could be achieved by integrating an in-line sensor with a mathematical model. It is therefore advantageous to develop reliable dissolution models that are capable of predicting the dissolution rate of the API based on its properties such as particle size distribution. Population balance equation could be a useful tool to predict the dissolution rate based on particle size distribution for products, if the particle size distribution has been established as a critical quality attribute for the product.

The population balance equation describes the nucleation, growth, aggregation/ agglomeration and breakage. Population balance equations can be formulated using an Eulerian or a Lagrangian approach, where the Lagrangian viewpoint tracks a finite number of particles in a flow field, while the Eulerian viewpoint tracks the particles as a bulk continuous phase [29]. These equations can be applied in the determination of dissolution rate and could be combined with an in-line particle size distribution measurement technique to enable real-time prediction of dissolution rates.

Given the significant results achieved with the technology introduced by Ficzere et al. [26] where the powder blends were transferred onto a conveyor belt and images were analysed using bounding boxes, a setup in which the blend is examined directly at the feeder output, making it possible for an ideal in-line application, along with the use of instance segmentation, could lead to notable advancements in determining particle shape and size distribution. The determined distribution could be combined with population balance equations to achieve real-time dissolution rate prediction.

2. Materials and methods

2.1 Materials

The model API used in the study, acetylsalicylic acid (ASA) was acquired from Sigma-Aldrich (St. Louis, Missouri, USA). Anhydrous calcium hydrogen phosphate (CHP) was obtained from JRS Pharma (Rosenberg, Germany). Microscopic images of the used materials are presented in Fig. 1. The presented images illustrate the differences between the two components in terms of shape (CHP being more circular), size (CHP having a smaller diameter) and transparency (ASA being more transparent).

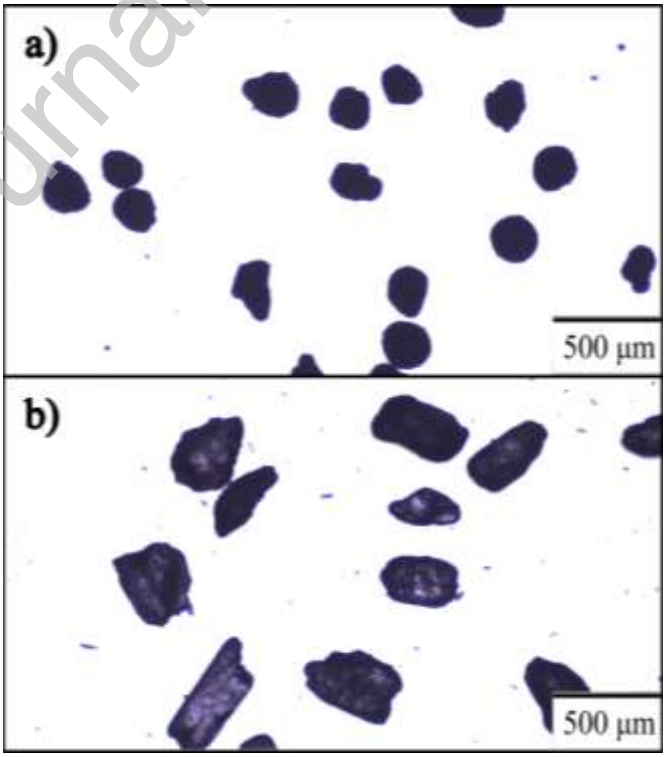

Fig. 1. Microscopic images of a) CHP b) ASA.

2.2 Methods

2.2.1 Preparation of powder blends

Sieving was performed for both ASA and CHP to obtain fractions. The CHP fraction consisted of particles that did not pass through the 200 µm diameter sieve. The three ASA fractions were obtained using two sieves, with particles that did not pass through the sieve with the smaller diameter being collected. The sieve pairs employed had the following diameters: 63-100 µm, 150-200 µm, and 300-500 µm. A CISA BA200N Compact Digital Electromagnetic Sieve Shaker (Barcelona, Spain) was used for sieving and the process was continued until the mass of material on the sieves no longer changed.

Sieving was followed by creating the blends of ASA and CHP. This was performed by manual rotation for 5 minutes in small plastic containers. Each contained 50 g of powder and the API concentration was 20% w/w in all samples. The composition of the three blends is presented in Table 1.

Table 1. The sieve fractions used in the three blends.

	ASA	**CHP**
Blend 1	150-200 µm	>200 µm
Blend 2	63-100 µm	>200 µm
Blend 3	300-500 µm	>200 µm

2.2.2 Real-time capture of images and videos

The powder blends were loaded into a twin-screw feeder (Brabender Technologie, Duisburg, Germany), which operated at a mass flow rate of 0.12 kg/h. The particles then fell onto a glass plate, which was inclined at a 45° angle to facilitate powder flow while maintaining the particles in the same plane. The 12-megapixel Basler acA4112-30uc (Basler, Ahrenberg, Germany) camera was positioned over the glass plate at a 90° angle. The objective attached to the camera was a 1.0X-3.0X VariMagTL telecentric objective (Edmund Optics, Barrington, New Jersey, USA), operating at the 3X magnification setting. The appropriate lighting was achieved using a high-intensity fiber optic LED light source, at an approximately 30° angle relative to the glass plate, which made the particles stand out from the background, making them more recognisable. A total of 812 images (resolution: 4096x3000) were captured of Blend 1, which were later used for the training of the object detection algorithm. Furthermore, 20-second videos were recorded of all three blends with a frame rate of 10 frames per second, which were later used for the determination of particle size distribution. The measurement setup is presented in Fig. 2.

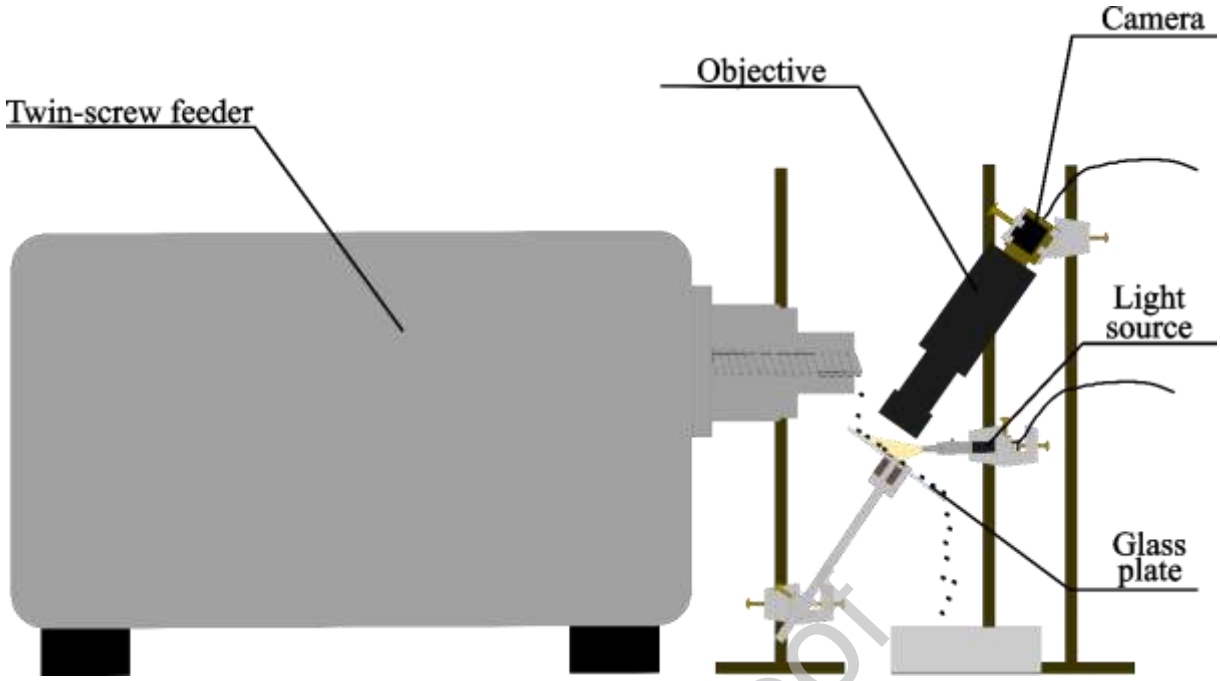

Fig. 2. Setup for real-time imaging of powder blends during continuous feeding.

2.2.3 Training of the YOLOv5 algorithm for particle and component recognition

The first step in the training of the YOLOv5 algorithm was the manual annotation and classification of particles, providing a reference pattern for the algorithm. Roboflow [30] was used for the manual annotation of objects (particles). It was essential to only annotate particles that were clearly distinguishable from the background and had well-defined edges. For this purpose, the Instance Segmentation function of Roboflow was used. Manual annotation was performed on the 812 images captured of Blend 1, images of Blends 2 and 3 were not used for training the model. The ASA and CHP particles were categorized into two different classes. A raw image and its annotated version are presented in Fig. 3.

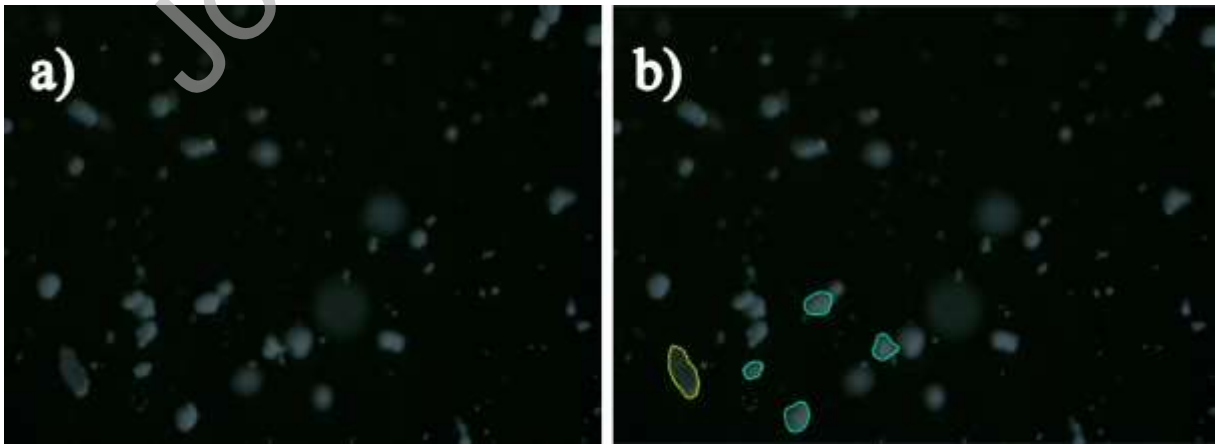

Fig. 3. Raw image of Blend 1 (a) and its manually annotated version (b) containing one ASA and four CHP particles that are properly visible.

The YOLOv5 model was then trained in Google Colab, using the manually annotated images, which were split into datasets for training, validation and testing. The number of images in each dataset is shown in Table 2. In the 568 training images, a total of 2008 CHP particles and 130 ASA particles were annotated. Although the overrepresentation of one class is not optimal, in this case, it did not lead to any issues in the training or in the subsequent size distribution determination.

The training of YOLOv5 was conducted over 200 epochs, while the dataset was split into batches, with a size of 10 images. As the training was completed, the file containing the weight factors of the developed model was saved for later utilization. The model had a P value of 0.842 and an R value of 0.707. P value stands for precision metric (Eq. (1)) and can be calculated using the number of true positives (TP) and false positives (FP). High precision indicates that the model's classifications are typically accurate, whereas a low precision value suggests that incorrect classifications occur frequently.

$$Precision = \frac{TP}{TP + FP} \tag{1}$$

Recall measures the model's effectivity in identifying all positive instances within the dataset. A high recall value indicates that the model successfully detects most instances of the target object, whereas a low value suggests frequent failures in object recognition. Recall can be calculated using Eq. (2), where FN stands for false negative [25].

$$Recall = \frac{TP}{TP + FN} \tag{2}$$

Table 2. The number of images in each dataset.

	Number of images in the dataset
Training	568
Validation	164
Testing	80

2.2.4 Determination of particle size distribution

The trained YOLOv5 model was used on the 20-second videos recorded of all three blends. The model was capable of recognizing and classifying the particles on frames that had not been annotated beforehand. After the object detection was performed by the model, the relative coordinates and other parameters of the detected particles were downloaded as text files, each belonging to an individual image.

The evaluation of this data was accomplished in MATLAB R2023b (Mathworks, Natick, Massachusetts, USA) with a custom-made code. Using the minimal Feret-diameter of each detected particle, the code calculated the number-based and volume-based particle size distribution of the components. The number-based distribution was used during the dissolution prediction described in Chapter 2.2.6. The more generally applied volume-based distribution was used for evaluating the performance of the real-time imaging system by comparing the distribution to the reference method described in Chapter 2.2.5.

The same method was performed on all three 20-second videos, captured of the different powder blends.
A 20-second video consists of approximately 200 frames. Assuming an average of 3-5 properly visible particles per frame, the analysis of each video examines around 600-1000 particles.

2.2.5 Reference method for particle size measurement

As a validation of the developed technology, images of each fraction were individually captured using a light microscope. Light microscopy was used as the reference method because it allows for the direct measurement of the minimum Feret diameter of the particle, which is not possible with techniques such as laser diffraction. An additional advantage of this method is its ability to directly determine particle size, whereas laser diffraction provides an indirect measurement. The images (resolution: 4912x2762) were acquired with an Olympus BX40 (Shinjuku City, Tokyo, Japan) light microscope, using a 4x zoom objective. For sample preparation, the particles of each fraction were dispersed on glass plates, with efforts made to minimize overlapping and contacting particles. Images were captured of the four fractions individually. The particles in the images were manually annotated using Roboflow. Roboflow annotation was employed to ensure that overlapping or contacting particles were not annotated, as an algorithm based on grey-level thresholding would have identified them as a single particle. Subsequently, the custom-made MATLAB code utilized the text files containing the parameters of the annotated particles to calculate their size distribution. This served as the reference for the results obtained with the developed method. Fig. 4 shows images of the four different fractions captured with light microscope.

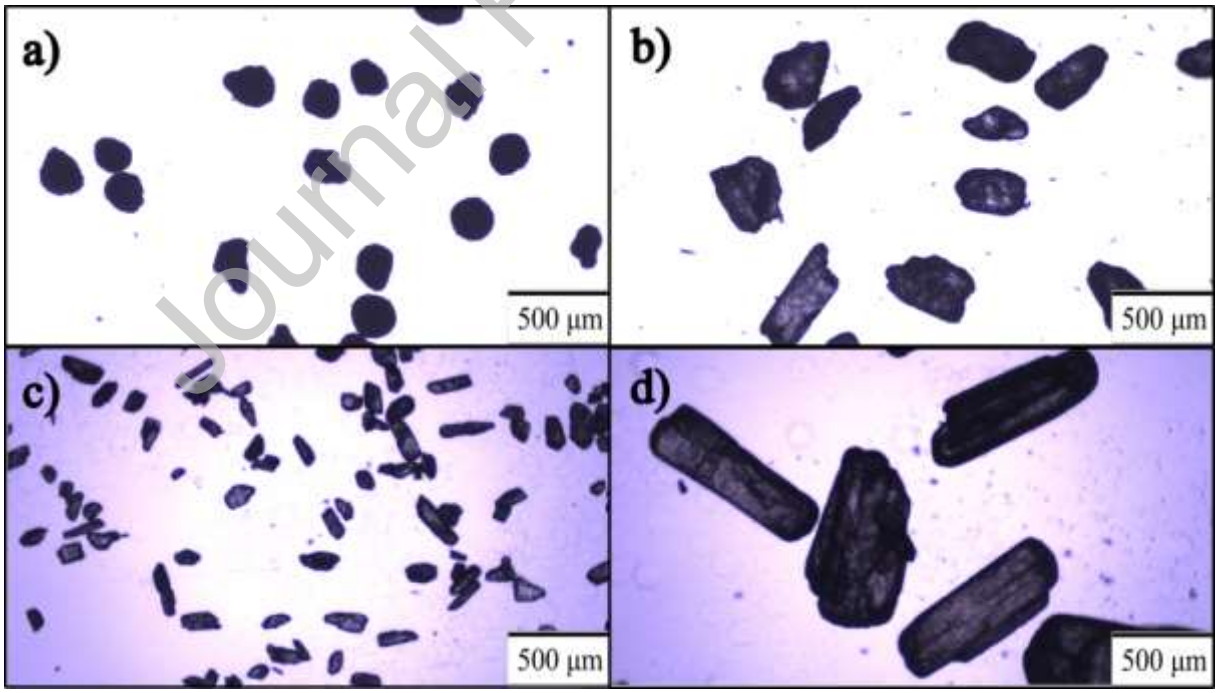

Fig. 4. Microscopic images of a) >200 µm CHP b) 150-200 µm ASA c) 63-100 µm ASA d) 300-500 µm ASA

2.2.6 Kolmogorov-Smirnov test

Two-sample Kolmogorov-Smirnov test was used to compare the particle size distributions obtained with the two different methods. The null hypothesis of the test was that the distributions obtained with the reference method and the real-time machine vision method came from the same distribution. The confidence level was 95%. The test returns two values. The h value is 1 if the null hypothesis is rejected and 0 if the null hypothesis is not rejected. The p value is the probability that the test statistic is as extreme as or, more extreme than, the observed value under the null hypothesis.
Table 3 presents the number of analysed particles for the real-time analysis. while the number of analysed particles for the microscope reference method is shown in Table 4.

Table 3. The number of analysed particles for the real-time analysis.

	CHP	ASA
Blend 1	996	76
Blend 2	1103	406
Blend 3	1178	15

Table 4. The number of analysed particles for the microscope reference method.

	CHP	150-200 µm ASA	63-100 µm ASA	300-500 µm ASA
Number of analysed particles	210	177	910	65

Based on [31], the use of the Kolmogorov-Smirnov test is not recommended for sample sizes below 30, but it is considered reliable for sample sizes above 50. In our case, with the exception of one sample, all our sample sizes exceed 50, leading us to deem the Kolmogorov-Smirnov test appropriate for our analysis. The small number of ASA particles was caused by the fact that in the case of 300-500 µm particle size, the mass is concentrated in a small number of large particles. We find it remarkable that even with such a small sample size, the real-time method yielded a relatively accurate measurement. To obtain more reliable results, mixtures with a large API particle size need to be monitored for a longer time so that more particles can be included in the analysis. From the perspective of the practical applicability of the developed method, this is not expected to pose a major problem, as API particles of this size are typically not used in industrial applications. However, our method can detect such particles if they occur as a result of some manufacturing problem.

2.2.7 In vitro dissolution measurement

From each of the three powder blends four capsules were prepared, each containing 150 mg of powder. Hard gelatine capsule shells (size 0) were used. On the capsules containing powder blends with identical fractions, parallel dissolution measurements were performed over a period of 120 minutes, with automated sampling at predetermined intervals (5, 10, 15 and 20 min, and afterwards every 10 min until 120 min) using a Hanson SR8-Plus dissolution tester (Chatsworth, CA, USA). The measurement was carried out in the USP II setting (paddle

method). The rotation speed of the paddles was 50 rpm, and spiral sinkers were used to ensure that the capsules stay at the bottom of the vessel. The medium was 900 mL of pH 1.2 HCl solution, tempered at 37°C. The concentration of ASA in the solution was measured using an Agilent 8453 on-line UV spectrometer (Hewlett-Packard, Palo Alto, CA, USA) by measuring the absorbance at 277 nm.

2.2.8. Prediction of the in vitro dissolution profile with population balance method

For the mathematical description of the dissolution a population balance model (PBM) was used. In this, the temporal evolution of the population density function and the concentration in the dissolution medium was described using differential equations combined with mass balances. It was assumed, that the temporal evolution of the population density function is only affected by the dissolution of the particles. A size-dependent dissolution rate equation was formulated, incorporating relative supersaturation and size effects, though supersaturation was considered insignificant under experimental conditions. The model was then solved using a high-resolution finite volume method, with parameters optimized by minimizing the root mean square error (RMSE) between experimental and simulated concentration data. The dissolution model assumed that capsule shell effects were constant, with ASA dissolution primarily influenced by particle size, and incorporated this by applying a constant retarding factor to the dissolution rate. The modelling methodology is described in detail in the work of Nagy et al. [32] . The PBM was developed in MATLAB R2024a (MathWorks, Natick, MA, USA). For the fitting of the PBM based on the measured ASA number-based particle size distributions of 63-100 µm and 300-500 µm samples were used, while the blend with 150-200 µm ASA fraction was used as validation.
The predicted and the measured dissolution were compared using the f_1 and f_2 parameters. The f_1 (difference factor) measures the percent error between two curves over the time points, while the f_2 (similarity factor) is a logarithmic transformation of the sum-squared error of differences between the test and reference products over the time points [33]. In the pharmaceutical practice, the similarity between the two curves is considered acceptable if the f_1 value is below 15 and the f_2 value exceeds 50.

3. Results and discussion

3.1 Results obtained with the microscopic analysis reference method

The results obtained with the off-line microscopic analysis correlated well with the expectations based on the sizes of the sieves used in the making of the ASA fractions. The CHP fraction's particle size distribution measured with the reference method was lower than expected. This could be attributed to the inefficiency of the sieving process. If the sieving was performed for a relatively short period or if CHP particles stuck in the apertures of the 200 µm diameter sieve, it could result in smaller particles being prevented from passing through the 200 µm sieve. The unexpectedly small particle size of CHP provides a great opportunity for testing our method. If our real-time method measures a similarly small particle size, then it demonstrates the capability of the newly developed tool. The reference particle size distributions of the fractions, obtained with the microscopic analysis, are shown in Fig. 5.

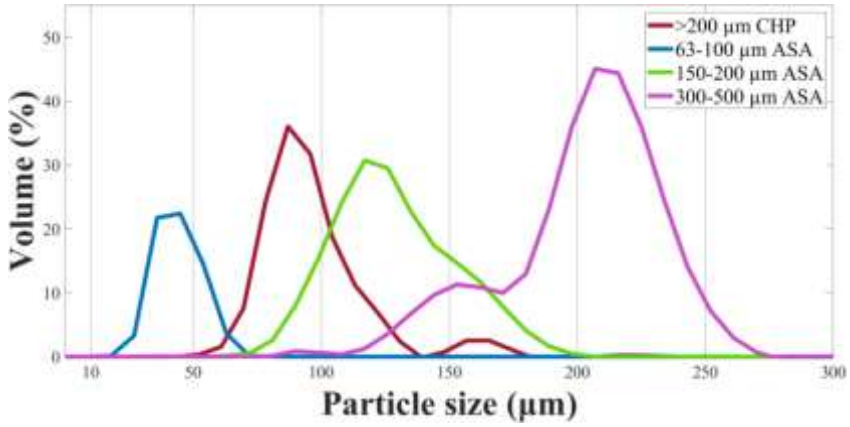

Fig. 5. Particle size distributions of the fractions measured with the microscopic analysis.

3.2 Evaluation of real-time videos and comparison of results from the developed and the reference method

The method outlined in the *Chapter 2.2.4.* was applied to all three 20-second videos captured of the powder blends. The particle size distributions, based on minimum Feret diameter, calculated using the developed method are compared with the results for the same fractions obtained from the microscopic reference method and presented in Fig. 6.

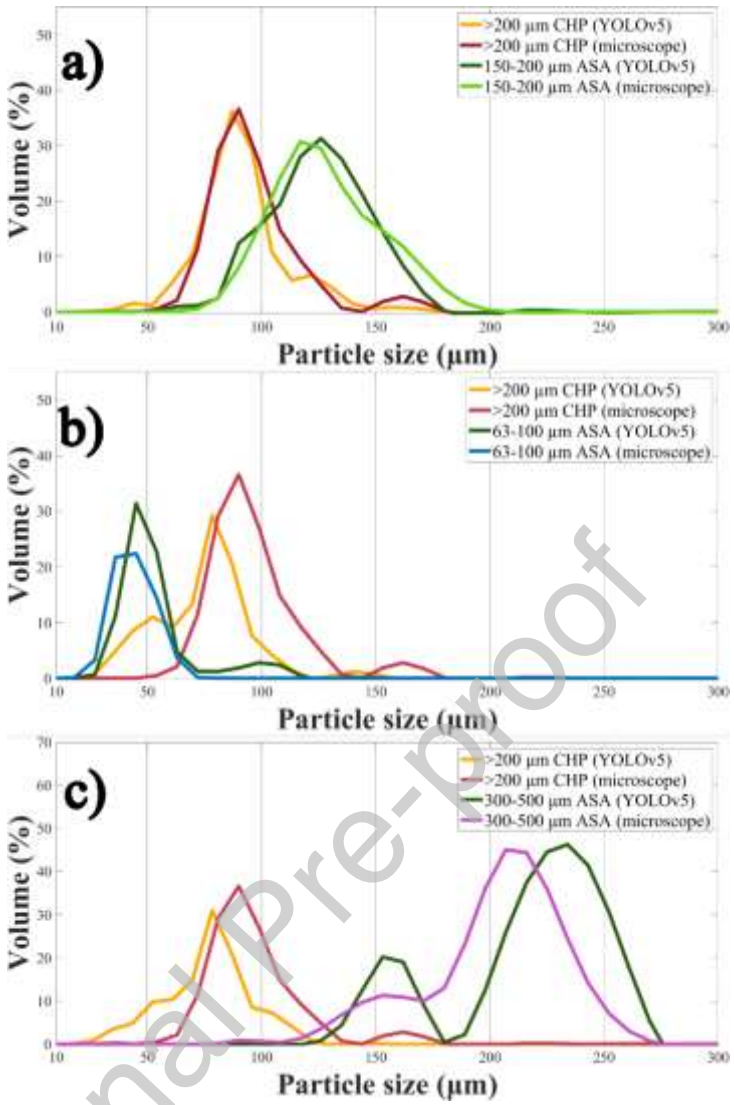

Fig. 6. Comparison of the minimum Feret diameter-based particle size distributions measured using the developed method and the reference method for a) Blend 1 (150-200 µm ASA) b) Blend 2 (63-100 µm ASA) c) Blend 3 (300-500 µm ASA).

The figures indicate that the results measured with the real-time machine vision method exhibit a high degree of similarity with the reference method. The curves obtained with the real-time machine vision method are very similar in the case of Blend 1. In the case of Blend 2, the two methods measured the size of ASA with only a slight difference. The size of CHP in Blends 2-3 and ASA in Blend 3 show larger differences. However, the real-time measurements still capture that the size of ASA is remarkably different compared to Blend 1. It should be noted that the YOLO model was trained using only images of Blend 1. Therefore, augmenting the training dataset with smaller and larger ASA particles would likely result in more accurate measurements in the case of the other size fractions. Overall, the results demonstrate the versatility of the new technology. In all three cases, the unexpectedly small size distribution of the CHP fraction measured with the real-time machine vision method correlated well with the distribution obtained using the reference method. For a more in-depth

comparison, D10, D50, D90, and span values were calculated using the results obtained from both methods. This comparison is presented in Table 5.

Table 5. D10, D50, D90, and span values calculated from the results obtained using the real-time machine vision method and reference method.

		Blend 1 (150-200 µm ASA; >200 µm CHP)		**Blend 2 (63-100 µm ASA; >200 µm CHP)**		**Blend 3 (300-500 µm ASA; >200 µm CHP)**	
		ASA	CHP	ASA	CHP	ASA	CHP
D10 (µm)	Reference method	96.46	75.05	32.11	75.05	145.52	75.05
	Real-time machine vision method	91.54	65.93	35.88	43.53	151.27	45.29
D50 (µm)	Reference method	122.48	90.94	41.99	90.94	204.23	90.94
	Real-time machine vision method	121.68	87.85	47.89	72.93	213.39	74.97
D90 (µm)	Reference method	159.79	113.76	55.15	113.76	239.49	113.76
	Real-time machine vision method	150.12	111.58	62.46	93.58	250.17	96.34
Span (-)	Reference method	0.52	0.43	0.55	0.43	0.46	0.43
	Real-time machine vision method	0.48	0.52	0.56	0.69	0.48	0.68

The high grade of similarity in the values proves the effectiveness of the developed method. This outcome was accomplished by training solely on images captured of Blend 1, without any prior exposure to data from the other two blends. This achievement is particularly notable given that in Blend 1 CHP and ASA particles had similar sizes, while in Blend 2 and Blend 3 the sizes of the two components differed more significantly. Although, as shown in Fig. 4 (images c) and d)), the size of ASA particles in Blend 2 and 3 differed significantly, the particle size distribution of ASA was effectively measured in both of these blends, demonstrating the technology's efficiency. This implies that the object detection model has good generalization ability and it does not differentiate between the particles based on only their size.

Our results are also significant considering that the similar method developed by Ficzere et al [26] was not able to recognize particles smaller than 100 µm, while our method successfully measured the particle size distribution of fractions that passed through a 100 µm sieve. In their study, the difference between the curves measured with the machine vision and the reference methods is visibly larger. This difference could stem from the distinction between bounding boxes and instance segmentation. Since our method uses instance segmentation, it can more accurately determine the outline of a particle, enabling more precise measurements. The developed technology was capable of calculating the component-based particle size distribution of powder blends, using real-time videos captured of the blends. This underscores the method's in-line efficiency in differentiating between different components and determining their individual particle size distributions – capabilities not previously achieved by other methods. A similar technology was introduced by Péterfi et al. [34], in which particle size was analysed during the pellet layering process using an artificial intelligence-based machine vision system. The method proved effective for in-line particle size analysis; however, in that setting, there was no need to differentiate between two classes of particles. Other studies, such as [35] and [36], have introduced methods using image-analysis for determining particle size distribution. With these methods the particle size distributions of the different components are measured separately and neither method was capable of measuring component-based particle size distribution in powder blends.

The possible limitations of the method include the lower efficacy of distinguishing components that show a high degree a similarity in their visual appearance. The lower limit of the minimal Feret diameter, at which the method is still able to adequately recognize and measure a particle, is unclear. Additionally, if an image contains a high density of particles, the method's efficiency in differentiating individual objects may decrease due to overlapping. The null hypothesis, according to the p values of the two-sample Kolmogorov-Smirnov tests, was not rejected for either of the distributions. This implies that there is no statistically significant difference between the particle size distribution obtained with the real-time machine vision method and the reference method. The results of the Kolmogorov-Smirnov test are shown in Table 6.

Table 6. The p and h values from the Kolmogorov-Smirnov tests.

	Blend 1 (150-200 µm ASA; >200 µm CHP)		**Blend 2 (63-100 µm ASA; >200 µm CHP)**		**Blend 3 (300-500 µm ASA; >200 µm CHP)**	
	ASA	CHP	ASA	CHP	ASA	CHP
p value from Kolmogorov-Smirnov test	0.5886	0.1625	0.3320	0.3874	0.4622	0.3481
h value from Kolmogorov-Smirnov test	0	0	0	0	0	0

3.3 Evaluation of the dissolution rates predicted with the PBM

The dissolution profiles of capsules containing the three powder blends are presented in Fig. 7.

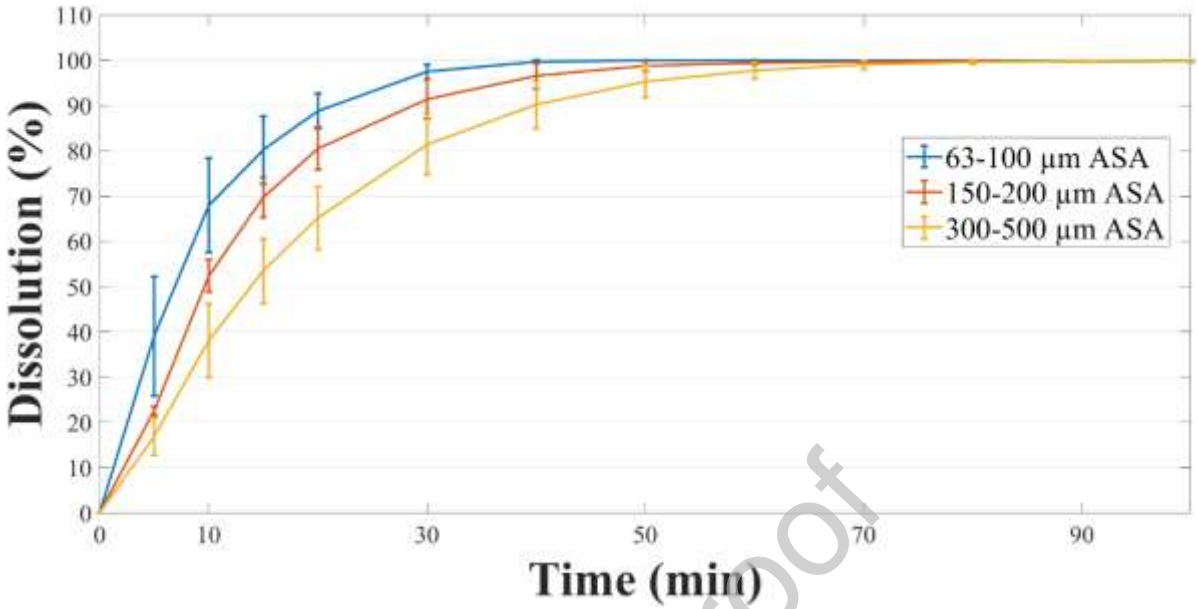

Fig. 7. The average and the standard deviation values of the four parallel measurements of capsules containing the three powder blends at the sampling time points.

As Fig. 7 shows, the particle size distribution and dissolution rate of the ASA correlated, with larger particles resulting in slower dissolution and smaller particles leading to faster dissolution.

The results from blends containing ASA fractions of 63-100 µm and 300-500 µm were used to fit the PBM's empirical parameter k_d. The model fitting resulted in a dissolution rate coefficient, $k_d = 4.6395*10^{-8}$. Afterwards, the particle size distribution of ASA in Blend 1 (150-200 µm) was used as input in PBM and the model was used to predict its dissolution profile. This enabled the validation of the model.

Fig. 8 shows how the fitted PBM predicted the dissolution rate of ASA in each size range, compared to the results obtained from the in vitro dissolution measurements.

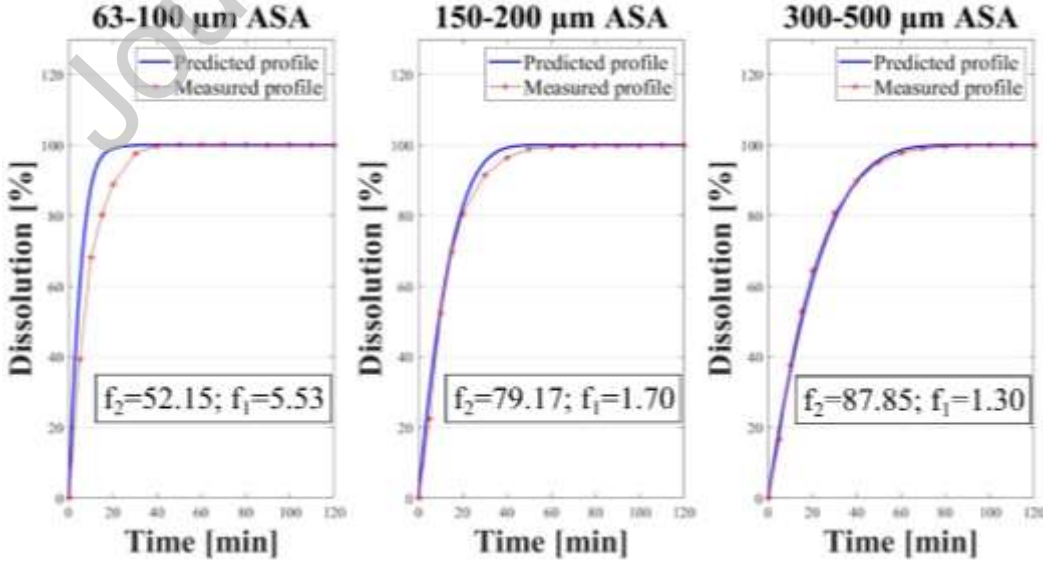

Fig. 8. The dissolution profiles predicted by the PBM method compared to the results of the in vitro dissolution measurements.

While n=12 data for both test and reference batches are a prerequisite for f_1/f_2 calculations, the smaller data pool we used should not be an issue, considering that this is a scientific paper. In the f_1/f_2 calculations all of the time points were included. In pharmaceutical quality control, only the time points preceding 85% of the maximum dissolution are considered. However, in our case, these values were used for a quantifiable comparison of the two curves. As illustrated in Fig. 8, the f_1 and f_2 values were within the acceptable range in all cases, demonstrating the model's efficiency. The similarity of the model's predictions and the measured values was lower for the blend containing ASA in the 63-100 μm size range, potentially indicating a limitation in predicting the dissolution rate for smaller particles. It is possible that smaller particles aggregate and consequently their specific surface area becomes smaller, leading to slower dissolution. The blend containing ASA in the 150-200 μm size range was used for validation. In that case both f_1 and f_2 values confirm the high efficiency of the PBM. It underscores the model's ability to predict the dissolution rate of the API using real-time particle size distribution data obtained with the novel real-time machine vision method. A paper by Kevin C. Johnson [37] discusses and compares different approaches to predicting dissolution based on particle size distribution. This demonstrates that there are existing methods capable of predicting dissolution profiles based on particle size distribution. Our work represents a step forward, as it combines an effective technology for determining component-based particle size distribution in powder-blends, with a model that uses the measured distribution to predict the dissolution profile of the API. Although it should be noted that the PBM, used for the mathematical description of dissolution profiles, can only be applied if dissolution is solely influenced by the API characteristics (e.g. particle size and solubility). Zaborenko et al. [38] describes two types of approaches to predictive dissolution modeling, first-principles approaches and empirical approaches. First-principles (physical) models predict drug dissolution based on fundamental physical and chemical properties, even before experimental testing. Empirical models use statistical and data-driven methods, such as linear regression and chemometric techniques, to predict dissolution based on formulation and process data. Based on this description, our model is a first-principles model. Such models are rarely integrated with real-time sensors to predict product quality. Our method is similar to the one outlined by Horkovics-Kovats et al. [39], which predicts dissolution based on data obtained using a PAT sensor - an approach that has yet to be extensively described in the literature.

Conclusion

This paper presented a novel PAT system in which machine vision combined with artificial intelligence was used to determine the component-based particle size distribution of pharmaceutical powder blends using videos captured by a digital camera, and to predict the dissolution rate of these blends. The method proved effective in recognizing particles, distinguishing between two components, and calculating the components' particle size distributions individually. For this, real-time videos were used, underscoring the in-line applicability of the method. Based on the determined particle size distributions of the ASA fractions, the dissolution rates were effectively predicted with a PBM.

Our method could be applied to multi-component blends, enhancing its versatility of use. Although similar-looking components may be a limitation for the method, with the implementation of techniques such as UV illumination, components that appear similar under visible light could be distinguishable. The component-based recognition allows the method to be applied in API content determination, which, similarly to particle size analysis, could

significantly contribute to advancements in pharmaceutical quality assurance. If applied on an industrial scale, the use of high-performance computers could significantly increase the number of images the method can evaluate (100-150 fps) and reduce the time needed for the training of the model, enhancing its speed and effectiveness in real-time measurements. Since powder blends are usually a precursor in pharmaceutical production, the method's ability to measure component-based particle size distribution can be applied not only in capsule formulations but also in the production of granules and tablets. In the latter scenarios, the method could be a way of evaluating intermediate products and it could provide vital information about the expected quality of the end product. For instance, knowing the particle size of API in the powder that will be tableted can enable the prediction of tablet quality.

Declaration of Competing Interest

The authors declare that they have no known competing financial interests or personal relationships that could have appeared to influence the work reported in this paper.

Acknowledgement

The project was supported by the European Union project RRF-2.3.1-21-2022-00004 within the framework of the Artificial Intelligence National Laboratory. It was also supported by the EKÖP-24-3-BME-41, EKÖP-24-3-BME-103 and EKÖP-24-4-II-BME-44 New National Excellence Program of the Ministry for Culture and Innovation from the source of the National Research, Development and Innovation Fund. The project was supported by the Doctoral Excellence Fellowship Programme (DCEP) is funded by the National Research Development and Innovation Fund of the Ministry of Culture and Innovation and the Budapest University of Technology and Economics, under a grant agreement with the National Research, Development and Innovation Office.

References

1. Brubaker, J. and S. Moghtadernejad, *A Comprehensive Review of the Rheological Properties of Powders in Pharmaceuticals.* Powders, 2024. **3**(2): p. 233-254.
2. Goh, H.P., P.W.S. Heng, and C.V. Liew, *Comparative evaluation of powder flow parameters with reference to particle size and shape.* International journal of pharmaceutics, 2018. **547**(1-2): p. 133-141.
3. Fu, X., et al., *Effect of particle shape and size on flow properties of lactose powders.* Particuology, 2012. **10**(2): p. 203-208.
4. Shekunov, B.Y., et al., *Particle size analysis in pharmaceutics: principles, methods and applications.* Pharmaceutical research, 2007. **24**: p. 203-227.
5. Madarász, L., et al., *AI-based analysis of in-line process endoscope images for real-time particle size measurement in a continuous pharmaceutical milling process.* International Journal of Pharmaceutics, 2023. **641**: p. 123060.
6. Abdel-Hamid, S., F. Alshihabi, and G. Betz, *Investigating the effect of particle size and shape on high speed tableting through radial die-wall pressure monitoring.* International journal of pharmaceutics, 2011. **413**(1-2): p. 29-35.
7. de Silva, S.R., A. Dyrøy, and G.G. Enstad. *Segregation mechanisms and their quantification using segregation testers*. in *IUTAM Symposium on Segregation in Granular Flows: Proceedings of the IUTAM Symposium held in Cape May, NJ, USA June 5–10, 1999*. 2000. Springer.
8. Jakubowska, E. and N. Ciepluch, *Blend segregation in tablets manufacturing and its effect on drug content uniformity—A review.* Pharmaceutics, 2021. **13**(11): p. 1909.

9. Péterfi, O., et al., *UV–VIS imaging-based investigation of API concentration fluctuation caused by the sticking behaviour of pharmaceutical powder blends.* International Journal of Pharmaceutics, 2024. **655**: p. 124010.
10. Ma, Z., et al., *On-line Measurement of Particle Size and Shape using Laser Diffraction.* Particle & Particle Systems Characterization: Measurement and Description of Particle Properties and Behavior in Powders and Other Disperse Systems, 2001. **18**(5-6): p. 243-247.
11. Wiegel, D., et al., *In-line particle size measurement and agglomeration detection of pellet fluidized bed coating by Spatial Filter Velocimetry.* Powder Technology, 2016. **301**: p. 261-267.
12. Muhaimin, M., A.Y. Chaerunisaa, and R. Bodmeier, *Real-time particle size analysis using focused beam reflectance measurement as a process analytical technology tool for continuous microencapsulation process.* Scientific reports, 2021. **11**(1): p. 19390.
13. Merkus, H.G. and H.G. Merkus, *Laser diffraction.* Particle size measurements: Fundamentals, practice, quality, 2009: p. 259-285.
14. Jain, R., R. Kasturi, and B.G. Schunck, *Machine vision*. Vol. 5. 1995: McGraw-hill New York.
15. Hirschberg, C., et al., *Image-based artificial intelligence methods for product control of tablet coating quality.* Pharmaceutics, 2020. **12**(9): p. 877.
16. Yu, W., et al., *Prediction of bulk powder flow performance using comprehensive particle size and particle shape distributions.* Journal of pharmaceutical sciences, 2011. **100**(1): p. 284-293.
17. Soprana, M., A.C. Santomaso, and P. Facco, *Artificial vision system for the online characterization of the particle size distribution of bulk materials on conveyor belts*, in *Computer Aided Chemical Engineering*. 2018, Elsevier. p. 1667-1672.
18. Galata, D.L., et al., *Applications of machine vision in pharmaceutical technology: A review.* European Journal of Pharmaceutical Sciences, 2021. **159**: p. 105717.
19. Martin, D., *A practical guide to machine vision lighting.* Midwest Sales and Support Manager, Adv Illum2007, 2007: p. 1-3.
20. Hannan, M., T. Burks, and D.M. Bulanon, *A machine vision algorithm combining adaptive segmentation and shape analysis for orange fruit detection.* Agricultural Engineering International: CIGR Journal, 2009.
21. Seelaboyina, R. and R. Vishwakarma. *Different Thresholding Techniques in Image Processing: A Review*. in *ICDSMLA 2021: Proceedings of the 3rd International Conference on Data Science, Machine Learning and Applications*. 2023. Springer.
22. Vijayakumar, A. and S. Vairavasundaram, *Yolo-based object detection models: A review and its applications.* Multimedia Tools and Applications, 2024: p. 1-40.
23. Lu, B., et al., *An alternative rotating object detection method for rock particle size distribution analysis.* Powder Technology, 2024. **444**: p. 120059.
24. Lawal, O.M., *YOLOv5-LiNet: A lightweight network for fruits instance segmentation.* Plos one, 2023. **18**(3): p. e0282297.
25. Fazekas, B., et al., *Process analytical technology based quality assurance of API concentration and fiber diameter of electrospun amorphous solid dispersions.* European Journal of Pharmaceutics and Biopharmaceutics, 2024: p. 114529.
26. Ficzere, M., et al., *Image-based simultaneous particle size distribution and concentration measurement of powder blend components with deep learning and machine vision.* European Journal of Pharmaceutical Sciences, 2023. **191**: p. 106611.
27. Dizaj, S.M., et al., *Nanosizing of drugs: effect on dissolution rate.* Research in pharmaceutical sciences, 2015. **10**(2): p. 95-108.
28. Shekunov, B. and E.R. Montgomery, *Theoretical analysis of drug dissolution: I. Solubility and intrinsic dissolution rate.* Journal of pharmaceutical sciences, 2016. **105**(9): p. 2685-2697.
29. Omar, H.M. and S. Rohani, *Crystal population balance formulation and solution methods: a review.* Crystal Growth & Design, 2017. **17**(7): p. 4028-4041.
30. *Roboflow*. Available from: roboflow.com Last update: 2024.10.08.
31. Mishra, P., et al., *Descriptive statistics and normality tests for statistical data.* Annals of cardiac anaesthesia, 2019. **22**(1): p. 67-72.

32. Nagy, B., et al., *Dynamic flowsheet model development and digital design of continuous pharmaceutical manufacturing with dissolution modeling of the final product.* Chemical Engineering Journal, 2021. **419**: p. 129947.
33. Costa, P. and J.M.S. Lobo, *Modeling and comparison of dissolution profiles.* European journal of pharmaceutical sciences, 2001. **13**(2): p. 123-133.
34. Péterfi, O., et al., *Artificial intelligence-aided endoscopic in-line particle size analysis during the pellet layering process.* Journal of Pharmaceutical Analysis, 2025: p. 101227.
35. Igathinathane, C. and U. Ulusoy, *Machine vision methods based particle size distribution of ball-and gyro-milled lignite and hard coal.* Powder Technology, 2016. **297**: p. 71-80.
36. Frei, M. and F.E. Kruis, *Image-based size analysis of agglomerated and partially sintered particles via convolutional neural networks.* Powder Technology, 2020. **360**: p. 324-336.
37. Johnson, K.C., *Comparison of methods for predicting dissolution and the theoretical implications of particle-size-dependent solubility.* Journal of pharmaceutical sciences, 2012. **101**(2): p. 681-689.
38. Zaborenko, N., et al., *First-principles and empirical approaches to predicting in vitro dissolution for pharmaceutical formulation and process development and for product release testing.* The AAPS journal, 2019. **21**: p. 1-20.
39. Horkovics-Kovats, S., et al., *Raman-based real-time dissolution prediction using a deterministic permeation model.* International Journal of Pharmaceutics, 2022. **617**: p. 121624.

Graphical abstract